

# Polymer-stabilized liquid crystal microlens array with large dynamic range and fast response time

Hongwen Ren,<sup>1,\*</sup> Su Xu,<sup>2</sup> and Shin-Tson Wu<sup>2</sup>

<sup>1</sup>Department of Polymer-Nano Science and Technology, Chonbuk National University, Jeonju, Jeonbuk 561-756, South Korea

<sup>2</sup>College of Optics and Photonics, University of Central Florida, Orlando, Florida 32816, USA

\*Corresponding author: hongwen@jbnu.ac.kr

Received July 15, 2013; revised July 23, 2013; accepted July 23, 2013;

posted July 24, 2013 (Doc. ID 193864); published August 14, 2013

We report a polymer-stabilized liquid crystal (LC) microlens array with a large dynamic range and fast response time. The top substrate has a planar indium-tin oxide (ITO) electrode, while the bottom substrate has two patterned ITO electrodes for generating a fringing field and uniform longitudinal field. The fringing field is utilized to create the desired gradient refractive index profile in the LC/monomer layer, which is later stabilized by UV curing to form polymer networks. To tune the focal length, we apply a longitudinal field to change the lens shape. This microlens array offers several attractive features, such as large dynamic range, fast response time, and good mechanical stability. © 2013 Optical Society of America

OCIS codes: (160.3710) Liquid crystals; (010.1080) Active or adaptive optics; (220.3630) Lenses.

<http://dx.doi.org/10.1364/OL.38.003144>

The liquid crystal (LC) microlens array is an essential optical device that has widespread applications in image processing [1–11], beam steering [12,13], wavefront correction [14], and switchable 2D/3D displays [15,16]. Various approaches for fabricating a microlens array have been proposed. The common one is to create a gradient refractive index distribution among LC molecules either by an inhomogeneous electric field [1,2,7–9,12,15,16] or by an inhomogeneous LC morphology [3–6,10,11,13]. Hole-patterned electrodes have been commonly used for making circular LC lenses, while polymer-stabilized LC (PSLC) is preferred for obtaining an inhomogeneous LC morphology. However, technical challenges of these LC lenses remain. The focal length ( $f$ ) of an LC lens is inversely proportional to the refractive index difference ( $n_c - n_b$ ), where  $n_c$  and  $n_b$  are the effective refractive indices at the lens center and border, respectively. In an LC lens with a hole-patterned electrode, the generated fringing field can produce the largest refractive index gradient at an optimal voltage. Therefore,  $n_c - n_b$  can approach the intrinsic birefringence ( $\Delta n$ ) of the LC material, leading to the shortest possible focal length. However, due to the gradient of the fringing field, it is difficult to further tune the focal length to infinity even if the voltage keeps increasing. As a result, the lens's dynamic range is rather limited [1,8]. Although a PSLC lens can be actuated by a uniform electric field, its  $n_c - n_b$  is usually much smaller than  $\Delta n$ , since a large gradient distribution of LC domains is not preferred in the PSLC [3,5,13]. Otherwise, large LC domains would cause light scattering, nonuniform response, and mechanical instability.

In this Letter, we combine the unique advantages of hole-patterned electrodes and PSLC to demonstrate a microlens array using a ring-array-patterned electrode in a homogeneous cell. The fringing field generates a large gradient refractive index distribution in the LCs, which is later stabilized by the polymer network. As a result, the fabricated PSLC microlens can utilize the maximum intrinsic birefringence of the LC material and present the shortest possible focal length. The focal

length is tuned by a uniform longitudinal field. Since no photomask is employed during the UV polymerization process, the formed PSLC has a uniform morphology. Adding 10 wt. % diacrylate monomer to the LC host, our PSLC microlens array offers attractive features, such as fast response time, good stability, and weak light scattering in the visible spectral range.

Figure 1 depicts the microlens structure and fabrication procedures. The cell consists of two indium-tin oxide (ITO) glass substrates, whose inner surfaces are coated with a thin polyimide (PI) layer with antiparallel rubbing. The top electrode is continuous. As Fig. 1(a) shows, the bottom electrode is divided into two disconnected parts by etching a circular ring (white color): electrode 1 (purple color) and electrode 2 (blue color). The filled nematic LC and diacrylate monomer mixture has a homogeneous alignment [Fig. 1(b)]. When a voltage ( $V_f$ ) is applied between the top common electrode and bottom electrode 1, a symmetric but inhomogeneous fringing field is generated in the area above electrode 2. Hence, a

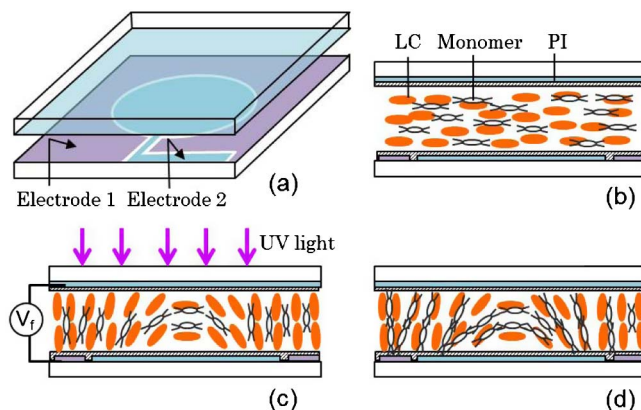


Fig. 1. Device structure and fabrication procedures of the proposed microlens array. (a) Device structure, (b) homogeneous alignment, (c) central-symmetrical gradient refractive index distribution introduced by the inhomogeneous fringing field and UV exposure, and (d) the formed PSLC microlens after removing the voltage.

gradient refractive index distribution is introduced there. After UV photopolymerization, the gradient refractive index distribution is fixed by the monomers [Fig. 1(c)]. Removing the voltage, such a distribution remains and the formed PSLC (in the area above electrode 2) exhibits a lens characteristic [Fig. 1(d)]. Its focal length can be tuned by applying a voltage between the top common electrode and bottom electrode 2. Since the generated electric field is uniform, the focal length of the PSLC lens can be tuned in a broad range.

In addition to a single lens, our approach also offers the ability to fabricate a PSLC microlens array in a relatively easy way. To prepare a PSLC microlens array, the bottom ITO electrode is patterned with a circular ring array. The inner and outer radii of the ring are 50 and 70  $\mu\text{m}$ , respectively. The distance between two adjacent rings is 30  $\mu\text{m}$ . The cell gap is  $\sim 15 \mu\text{m}$ . To enhance the polymer network stability and minimize light scattering, the Merck LC host BL-009 (birefringence  $\Delta n = 0.281$  and ordinary refractive index  $n_o = 1.529$  at  $\lambda = 589 \text{ nm}$  and  $20^\circ\text{C}$ , dielectric anisotropy  $\Delta\epsilon = 15.5$  at 1 kHz and  $20^\circ\text{C}$ , viscosity  $\eta = 83 \text{ cS}$  at  $20^\circ\text{C}$ ) was doped with  $\sim 10 \text{ wt.}\%$  RM257 (containing a small amount of photoinitiator). RM257 has a rod-like structure and can be easily aligned with the LCs. The mixture was thoroughly stirred and filled into the cell by capillary flow.

To investigate the impact of the fringing field on the gradient refractive index distribution of LCs, various voltages were applied between the top electrode and electrode 1, and the cell was observed by a polarizing optical microscope. The cell was placed between two crossed polarizers, with the rubbing direction  $45^\circ$  to the optic axis of the front polarizer. At  $V = 0$ , the LC/monomer presents a homogeneous alignment (under green light illumination,  $\lambda \sim 550 \text{ nm}$ ) [Fig. 2(a)]. When the voltage exceeds  $2.5 V_{\text{rms}}$ , interference rings begin to arise at the border of the hole-shaped electrode 1. As the voltage further increases, the interference rings expand toward the hole center. At  $V = 4 V_{\text{rms}}$ , more than four concentric circular rings are observed [Fig. 2(b)]. At  $V = 6 V_{\text{rms}}$ , the interference rings touch the hole center and more than six rings are observed, as shown in Fig. 2(c); the inset is the magnified inference pattern of one zone. At  $V = 7 V_{\text{rms}}$ , the interference rings becomes asymmetrical, as shown in Fig. 2(d), and the inset is the

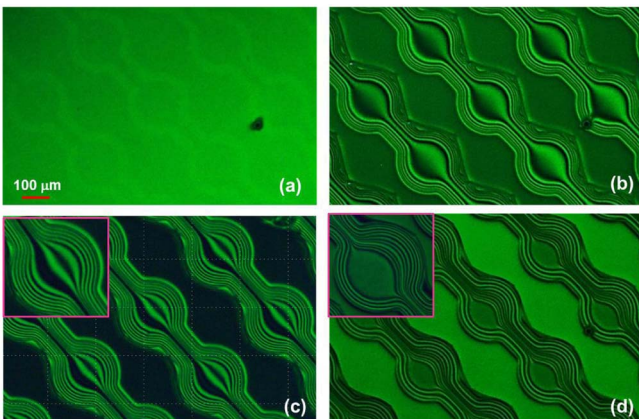


Fig. 2. Interference patterns of the cell at different voltages: (a)  $V = 0$ , (b)  $V = 4 V_{\text{rms}}$ , (c)  $V = 6 V_{\text{rms}}$ , and (d)  $V = 7 V_{\text{rms}}$ .

magnified inference pattern of one zone. The asymmetry is mainly caused by the fringing field distribution in the electrode 2 area. By optimizing the cell structure, such as the ratio between the cell gap and the inner diameter of electrode 2, the asymmetry can be minimized [17].

The LC/monomer mixture was then photopolymerized at  $V = 6 V_{\text{rms}}$ , the UV exposure ( $\lambda \sim 365 \text{ nm}$ ,  $\sim 10 \text{ mW/cm}^2$ ) lasting for 20 min. Removing the voltage, the observed interference pattern of the cell after UV exposure [Fig. 3(a)] is almost the same as that before UV exposure [Fig. 2(c)]. Such a result implies that the formed polymer network stabilizes the gradient orientation of the LC molecules well. When the rubbing direction of the cell is oriented parallel to the optic axis of the polarizer, a dark state is observed in each zone [Fig. 3(b)], indicating that the PSLC is optically anisotropic. Nevertheless, once the PSLC is formed, it is difficult to actuate by the fringing field. Instead, a uniform longitudinal electric field is adopted by applying a voltage ( $V_u$ ) between the top electrode and bottom electrode 2 [Fig. 3(c)]. When a voltage of  $120 V_{\text{rms}}$  is applied to the cell, the interference rings cannot be observed [Fig. 3(d)]. To visually observe the influence of a uniform electric field on the formed PSLC, a video ( $320 \times 240$ ) was recorded, which is provided in Fig. 3(d) (Media 1). In the video, we first increase the voltage from 0 to  $120 V_{\text{rms}}$  gradually and then decrease it to 0. As the voltage exceeds  $28 V_{\text{rms}}$ , the interference patterns begin to vanish. The cell shows a clear interference pattern change when the voltage increases from  $28 V_{\text{rms}}$  to  $90 V_{\text{rms}}$ . The number of interference rings decreases as the voltage increases. At  $V > 115 V_{\text{rms}}$ , all the interference rings vanish completely. Removing the voltage, the interference rings return to their original state. Although the interference pattern vanishes at  $V > 115 V_{\text{rms}}$ , the lens cell is not completely dark due to the weak scattering of PSLC in the visible region. With  $\sim 10 \text{ wt.}\%$  diacrylate monomer, the scattering is below 10% for the green light and diminishes as the wavelength increases to the

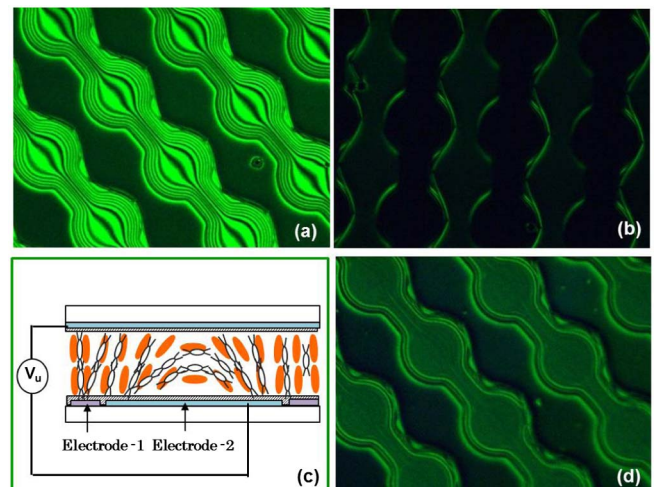


Fig. 3. (a) Observed interference pattern at  $V = 0$ , (b) dark state when the rubbing direction of the cell is parallel to the optical axis of polarizer at  $V = 0$ , (c) PSLC microlens array actuation, and (d) dynamic tuning of PSLC microlens array (Media 1).

near-IR region [18]. To further suppress light scattering, we could increase the polymer network density by increasing the monomer concentration or UV exposure intensity to reduce the LC domain size. In addition to reducing scattering, a small domain size also improves the response time. A trade-off is the increased operation voltage. Another way to eliminate scattering is to operate the device at a longer wavelength, e.g., near-IR or short-wavelength IR.

Similar to other PSLC lenses, here each zone showing a concentrically circular interference pattern exhibits a lens characteristic [Fig. 3(a)]. By orienting the rubbing direction of the PSLC cell parallel to the optic axis of the polarizer and removing the analyzer, we observed a 2D focus spot array through a microscope. The focus spots are quite circular, and there is no obvious noise in the dark background [Fig. 4(a)]. To investigate its imaging capability, we printed a small letter “A” on a transparency and placed it under the cell as an object. By readjusting the distance between the cell and the object, we observed a clear image of inverted “A” array [Fig. 4(b)]. It appears that the PSLC microlens suffers from astigmatism, which is caused by the birefringence of the LC material. It can be reduced by using a thinner LC layer [19] or minimized by selecting a specific shape factor of the LC lens [20]. However, this shape factor is significantly different from that for minimizing its spherical aberration and coma [20]. To balance all the possible aberrations arising in an LC lens, a proper shape factor should be chosen.

According to the dynamic video shown in Fig. 3(d), we can see that the focal length of each microlens is electrically tunable, evidenced from the fact that interference patterns can be changed by the voltage. The focal length is calculated based on the number of interference fringes, as expressed by

$$f = \frac{r^2}{2N\lambda}, \quad (1)$$

where  $r$  is the radius of the lens aperture,  $\lambda$  is the wavelength, and  $N$  is the number of the interference rings. The focal length at various voltages is estimated in Fig. 5. At  $V = 0$ , the shortest focal length is  $\sim 378 \mu\text{m}$  at  $\lambda \sim 0.55 \mu\text{m}$ . As the voltage increases, the focal length increases gradually. At  $V > 115 V_{\text{rms}}$ , the focal length is too long to be estimated.

Due to the high monomer concentration in the mixture, the formed polymer network is very rigid. Thus the dynamic response of our PSLC microlens is fast. We adopted a 633 nm laser (JDSU 1125P), photodiode

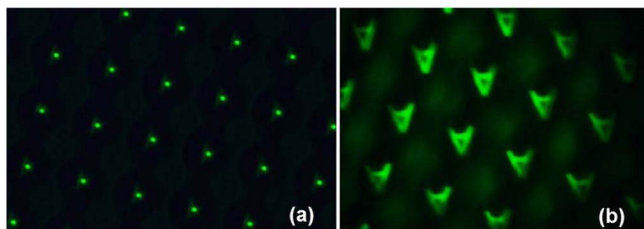


Fig. 4. (a) 2D focus spot array and (b) image of inverted “A” array.

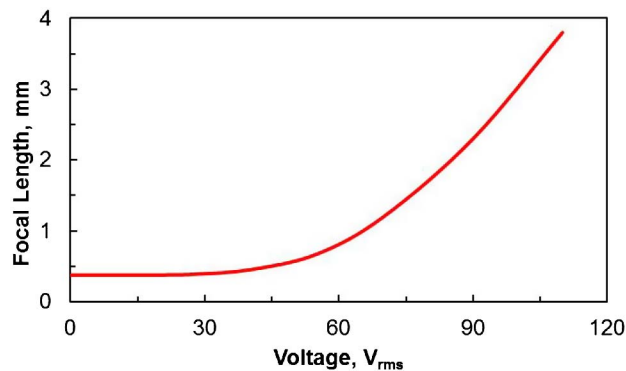


Fig. 5. Focal length versus external voltage applied to the cell.

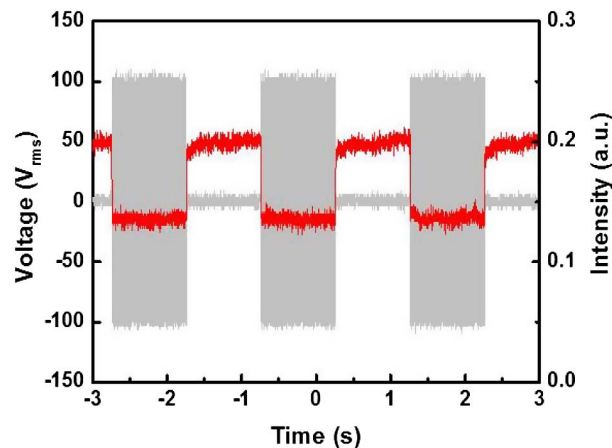


Fig. 6. Light intensity versus time. The amplitude of the voltage applied to the cell is a 100 V square pulse.

(Model 2031, New Focus), and oscilloscope (TDS 3032B, Tektronix) in our measurement. By focusing and defocusing the laser beam, the photodiode receives different light intensities. The intensity change with time can be analyzed using the oscilloscope. Using 100 V square voltage pulses to impact the cell, the  $\tau_{\text{rise}}$  (from focusing to nonfocusing) and  $\tau_{\text{fall}}$  (from nonfocusing to focusing) times were measured to be  $\sim 3.6$  and  $\sim 0.9$  ms, respectively, as shown in Fig. 6. The cycle driving with three periods shows that the PSLC microlens returns to its original state quite well. After a hundred cycles of continuous driving, the measured light intensity curve does not change. Such a result implies that our PSLC has good mechanical stability. The  $\tau_{\text{rise}}$  and  $\tau_{\text{fall}}$  under other three square voltage pulses were also measured, as listed in Table 1.

From Fig. 3(a), it can be seen that the interference rings formed in each zone are not closed. This is because the connecting electrode between the adjacent zones

Table 1. Measured Response Time under Various Square Voltage Pulses

Voltage (V)	$\tau_{\text{rise}}$ (ms)	$\tau_{\text{fall}}$ (ms)
60	5	0.79
80	4.1	0.83
100	3.6	0.9
120	2.9	1.28

also affects the orientation of LC molecules. Such cross talk distorts the interference patterns. Here the connecting electrode is quite wide (30  $\mu\text{m}$ ), so the induced cross talk greatly degrades the lens performance. Using a much narrower (<4  $\mu\text{m}$ ) connecting electrode, the cross talk can be significantly reduced.

In conclusion, we have demonstrated a novel PSLC microlens array in which the gradient refractive index distribution is controlled by a fringing field and the focal length tuned by a uniform longitudinal field. The dynamic range of each microlens is dependent on the fringing field applied to the cell during UV exposure. Optimizing the cell structure, such as the cell gap and the electrode 2 dimensions, our microlens can maximally utilize the intrinsic birefringence of the LC material and therefore present the shortest possible focal length, which approaches the theoretical limit. The cross talk induced by the connecting electrode can be significantly reduced if the electrode width is narrow enough. In comparison with a conventional LC microlens array, our PSLC microlens array offers a large dynamic range, fast response time, and good stability. It holds great potential for imaging, display, and biomedical applications, such as camera lenses, autostereoscopic 3D displays, pico projectors, and endoscopes.

H. Ren is grateful for the financial support of the National Research Foundation (NRF) of Korea under grant 2012-0004814. The UCF group is indebted to the U.S. Air Force Office of Scientific Research (AFOSR) for financial support under Contract No. FA95550-09-1-0170.

#### References

1. T. Nose, S. Masuda, S. Sato, J. Li, L.-C. Chien, and P. J. Bos, *Opt. Lett.* **22**, 351 (1997).

2. A. F. Naumov, M. Y. Loktev, I. R. Guralnik, and G. Vdovin, *Opt. Lett.* **23**, 992 (1998).
3. H.-S. Ji, J.-H. Kim, and S. Kumar, *Opt. Lett.* **28**, 1147 (2003).
4. Y. Choi, J.-H. Park, J.-H. Kim, and S.-D. Lee, *Opt. Mater.* **21**, 643 (2003).
5. H. Ren and S.-T. Wu, *Appl. Phys. Lett.* **82**, 22 (2003).
6. V. V. Presnyakov and T. V. Galstian, *J. Appl. Phys.* **97**, 103101 (2005).
7. M. Kawamura, M. Ye, and S. Sato, *Opt. Express* **16**, 10059 (2008).
8. Y.-H. Lin, H.-S. Chen, H.-C. Lin, Y.-S. Tsou, H.-K. Hsu, and W.-Y. Li, *Appl. Phys. Lett.* **96**, 113505 (2010).
9. Y.-Y. Kao, P.C.P. Chao, and C.-W. Hsueh, *Opt. Express* **18**, 18506 (2010).
10. M.-C. Tseng, F. Fan, C.-Y. Lee, A. Murauski, V. Chigrinov, and H.-S. Kwok, *J. Appl. Phys.* **109**, 083109 (2011).
11. L. Lu, V. Sergan, T. Van Heugten, D. Duston, A. Bhowmik, and P. J. Bos, *Opt. Express* **21**, 7133 (2013).
12. S. Masuda, S. Takahashi, T. Nose, S. Sato, and H. Ito, *Appl. Opt.* **36**, 4772 (1997).
13. J. Sun, S. Xu, H. Ren, and S.-T. Wu, *Appl. Phys. Lett.* **102**, 161106 (2013).
14. L. Hu, L. Xuan, D. Li, Z. Cao, Q. Mu, Y. Liu, Z. Peng, and X. Lu, *J. Opt. A* **11**, 015511 (2009).
15. J.-H. Na, S. C. Park, S.-U. Kim, Y. Choi, and S.-D. Lee, *Opt. Express* **20**, 864 (2012).
16. C.-W. Chen, Y.-P. Huang, and P.-C. Chen, *J. Display Technol.* **8**, 559 (2012).
17. T. Nose and S. Sato, *Liq. Cryst.* **5**, 1425 (1989).
18. J. Sun, Y. Chen, and S.-T. Wu, *Opt. Express* **20**, 20124 (2012).
19. H. Kikuta, K. Iwata, and H. Shimomura, *J. Opt. Soc. Am. A* **9**, 814 (1992).
20. J. P. Lesso, A. J. Duncan, W. Sibbett, and M. J. Padgett, *Appl. Opt.* **39**, 592 (2000).